Particle & Particle Systems Characterization
www.particle-journal.com

Gas-Generating, pH-Responsive Calcium Carbonate Hybrid Particles with Biomimetic Coating for Contrast-Enhanced Ultrasound Imaging

*Mark Louis P. Vidallon, Alon M. Douek, Adam Quek, Heather McLiesh, Jan Kaslin, Rico F. Tabor, Alexis I. Bishop, and Boon Mian Teo**

This work reports the fabrication of biocompatible and pH-sensitive hybrid polydopamine/bovine serum albumin/calcium carbonate (PDA/BSA/$CaCO_3$) particles via a rapid precipitation method. These hybrid particles generate hyperechogenic carbon dioxide bubbles upon exposure to low pH environments, making them ideal as a contrast agent and detector for tumor cells. This study also highlights the application of red blood cell membrane (RBC)-derived membranes as a biomimetic coating for PDA/BSA/$CaCO_3$ hybrid particles in order to modulate protein corona formation, a natural physiological response that alters tailored properties of most nanomaterials that are administered systemically. Results of this work demonstrate that the RBC membrane-coated hybrid particles are ideal for a wide range of biomedical applications, such as noninvasive multimodal imaging, photothermal and photodynamic therapy, and "personalized" drug delivery systems.

1. Introduction

Ultrasound imaging is one of the most powerful advancements in noninvasive, diagnostic imaging techniques that has allowed clinicians and researchers to probe and unravel delicate and difficult-to-access anatomical structures. This technique can provide valuable complementary information to other structural and functional imaging techniques, such as magnetic resonance imaging, computed tomography, positron emission tomography, and single-photon emission tomography for effective diagnostics.[1] However, compared with these other imaging techniques, ultrasound images are inferior in terms of image quality.[2] Furthermore, similarities in the echogenicities of tissues surrounding those of interest result in low contrast images. This may require the use of intravascular contrast enhancers, materials that exhibit large acoustic impedance and dissimilar compressibility to blood, in order to scatter ultrasound and generate images with more detailed features of the structures being scanned.[3]

Conventional ultrasound contrast agents comprise microbubbles. Microbubbles, usually formulated using lipids and other synthetic stabilizers, enhance ultrasound contrast by resonating with a specific frequency, which is dependent on the bubble diameter.[4] Microbubbles can be functionalized with biomacromolecules and inorganic compounds to respond to certain types of stimuli and can be localized to specific target tissues.[5] Recent advances in materials science have led to the development of solid-phase ultrasound contrast agents: inorganic particles that have high acoustic reflectivity; hollow particles that exhibit a stronger dynamic response compared to solid spheres; multilayer particles that exhibit multiscattering/reflection; and particles that generate bubbles upon exposure to stimuli.[6] Among these, biocompatible calcium carbonate ($CaCO_3$) particles can undergo decomposition to generate hyperechogenic carbon dioxide bubbles in acidic conditions, displaying potential as ultrasound contrast agents that can be triggered/activated under stereotypically low tumor extracellular pH.[7] For the same reason, $CaCO_3$ particles and combinations of these particles with polymeric and other inorganic materials have been studied intensively for their potential applications as pH-sensitive drug release and tumor detection systems.

One of the challenges of nanoparticle-based ultrasound contrast agents, and nanoparticles in general, is the

M. L. P. Vidallon, Dr. R. F. Tabor, Dr. B. M. Teo
School of Chemistry
Monash University
Clayton, VIC 3800, Australia
E-mail: boonmian.teo@monash.edu
A. M. Douek, Dr. J. Kaslin
Australian Regenerative Medicine Institute
Monash University
Clayton, VIC 3800, Australia
Dr. A. Quek
Department of Biochemistry and Molecular Biology
Monash University
Clayton, VIC 3800, Australia
H. McLiesh
BioPRIA
BioResource Processing Research Institute of Australia
Department of Chemical Engineering
Monash University
Clayton, VIC 3800, Australia
Dr. A. I. Bishop
School of Physics and Astronomy
Monash University
Clayton, VIC 3800, Australia
The ORCID identification number(s) for the author(s) of this article can be found under https://doi.org/10.1002/ppsc.201900471.

DOI: 10.1002/ppsc.201900471

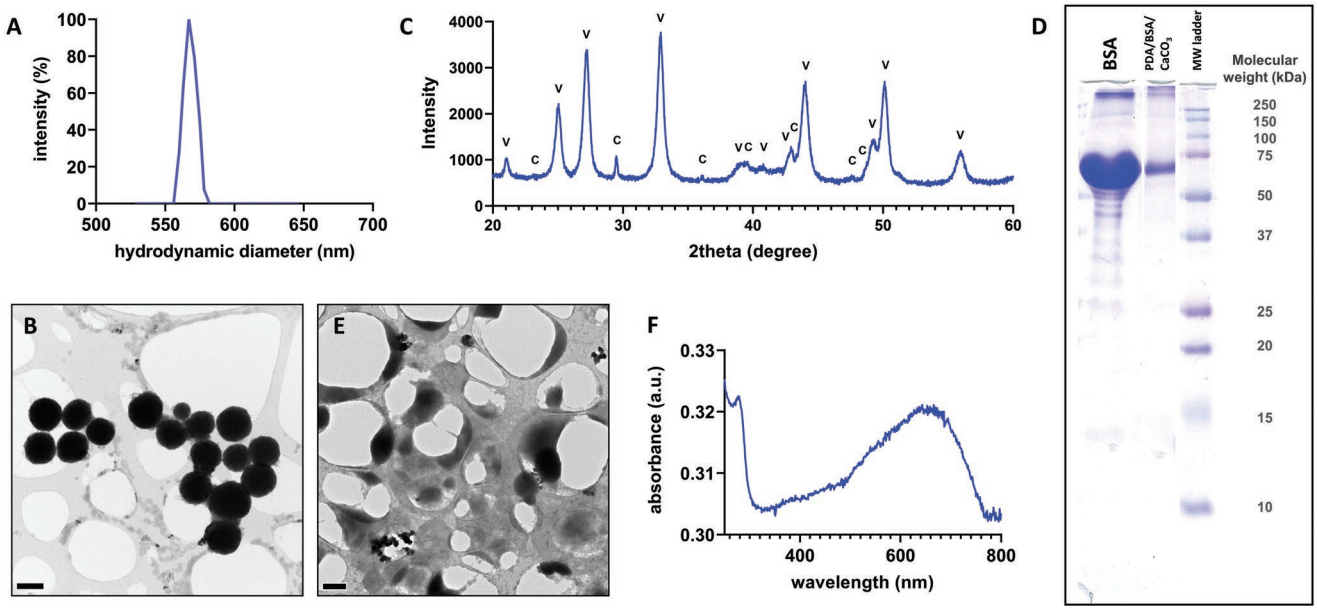

Figure 1. A) Particle size distribution, B) transmission electron image, and C) powder X-ray diffractogram of PDA/BSA/$CaCO_3$. Letters on the peaks in the diffractogram denote crystalline phase of $CaCO_3$: C = calcite and V = vaterite. D) SDS–PAGE analysis shows protein bands of BSA, PDA/BSA/$CaCO_3$, and standard protein molecular weight markers (MW ladder). E) Transmission electron image showing the PDA coating after etching $CaCO_3$ with 1.0 M HCl. Scale bars = 500 nm. F) UV–vis absorption spectrum of PDA/BSA/$CaCO_3$ dispersion.

formation of the hard protein corona upon lengthy exposure to systemic circulation. Adsorption of circulating proteins onto nanoparticles can alter the physicochemical properties (size, surface charge, surface composition, and functionality) of the material, conferring to these particles a new biological identity that determines their physiological response, including agglomeration, cellular uptake, circulation time, signaling, kinetics, transport, accumulation, and toxicity.[8] This may result in the particles displaying low response to stimuli as well as failure to reach, concentrate, and exert their action on their target sites. A novel way to circumvent this challenge is to apply biomimetic coating/cloaking technology using cell membranes, including erythrocytes, macrophages, thrombocytes, and lymphocytes. The complex biological composition of the cell membrane surface regulates the adsorption of biological components, facilitating longer circulation time, improved biocompatibility, and preventing immune-mediated degradation of particles.[9]

In this study, we fabricated polydopamine/bovine serum albumin/calcium carbonate (PDA/BSA/$CaCO_3$) hybrid particles and characterize important physicochemical properties, highlighting their possible application in contrast-enhanced ultrasound imaging. PDA can be obtained from the oxidative polymerization of the catecholamine neurotransmitter dopamine under basic conditions. This material is gaining popularity in a variety of applications due to its biocompatibility and excellent optoacoustic properties.[10] This work also demonstrates the application of red blood cell (erythrocyte) membrane coating technology on the PDA/BSA/$CaCO_3$ hybrid particles to inhibit hard protein corona formation in a simulated biological environment.

2. Results and Discussion

2.1. Preparation of PDA/BSA/$CaCO_3$ Hybrid Particles

$CaCO_3$ particles can be prepared using a variety of methods, including emulsion techniques, biomineralization, flame synthesis, reactive/chemical precipitation techniques,[11] and gas diffusion methods.[12] In this study, $CaCO_3$ hybrid particles were prepared by chemical precipitation, using $CaCl_2$ and Na_2CO_3 with BSA and PDA, yielding hybrid particles with an average hydrodynamic diameter of 572 nm (**Figure 1**A) and a polydispersity index of 0.253. Transmission electron microscopy (TEM) images (Figure 1B) show that the hybrid particles produced have a spherical shape with a spherulitic structure, a characteristic of the vaterite polymorph of $CaCO_3$.[13] However, X-ray powder diffractometry shows that the obtained nanoparticles are a mixture of the polymorphs vaterite and calcite (Figure 1C). Fourier transform infrared (FTIR) absorption bands (Figure S1, Supporting Information) corresponding to the functional groups of BSA and PDA presented very subtly due to the low amount of these materials and had to be confirmed using other methods. BSA acts as a regulator of particle growth by adsorbing onto the growing nanoparticle surface, which influences the size, morphology, and polymorph phase of the obtained $CaCO_3$ particles. BSA can coordinate with Ca^{2+}, increasing the local supersaturation around the protein, favoring the formation of the metastable polymorph vaterite. Retention of BSA in the hybrid particles, even after multiple washings, was confirmed by sodium dodecyl sulfate-polyacrylamide gel electrophoresis (SDS-PAGE) (Figure 1D). This may imply that BSA molecules have been adsorbed onto the surface of the formed particles or the nanograins comprising the

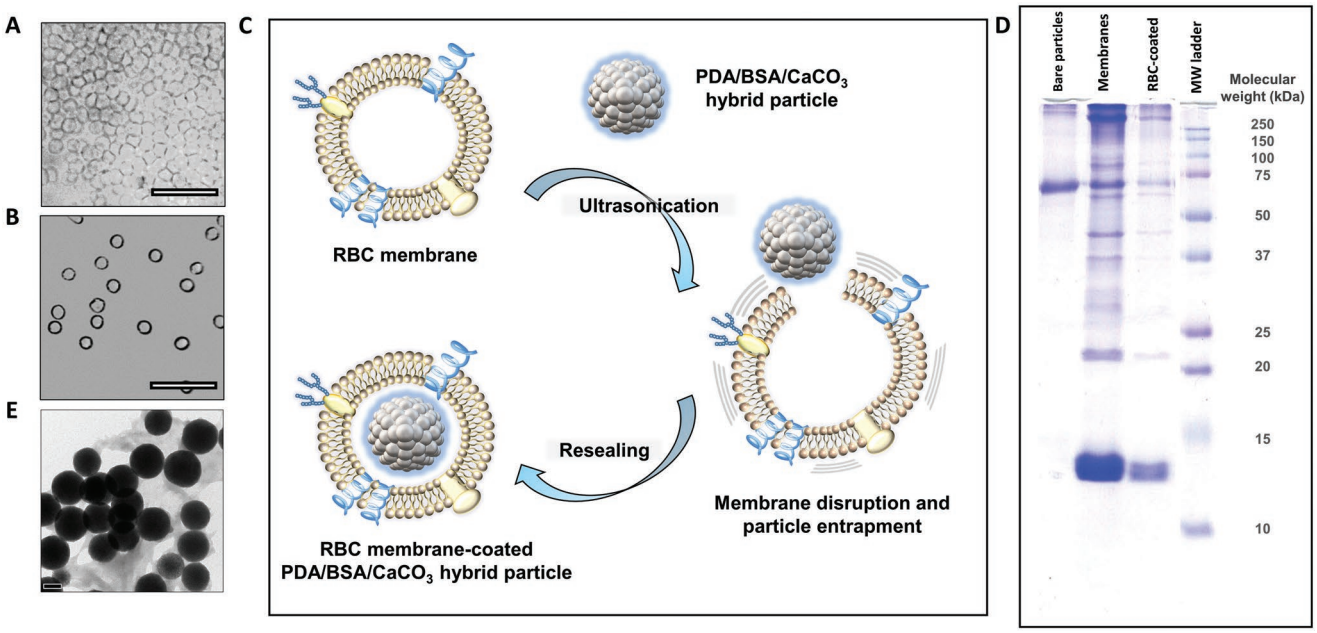

Figure 2. Optical microscopy images of A) RBC membranes derived from B) RBCs by hypotonic hemolysis. Scale bar = 25 µm. C) A schematic representation of the ultrasound-mediated coating of RBC membrane around the hybrid particles. D) SDS–PAGE analysis showing the protein bands of bare PDA/BSA/$CaCO_3$, RBC membranes, RBC membrane-coated PDA/BSA/$CaCO_3$, and standard protein molecular weight markers (MW ladder). E) Transmission electron image showing the morphology of RBC membrane-coated PDA/BSA/$CaCO_3$ hybrid particles. Scale bar = 500 nm.

spherulites, thus preventing the dissolution and limiting the growth of the particles.[14]

PDA is a dark-colored polymer produced by the oxidative polymerization of dopamine under basic pH conditions. Over decades, this polymer has been extensively studied in nanoparticle form, and as additives and coatings for surfaces and other nanostructures. Further, it is regarded as a biocompatible material with potential applications in the fields of photoacoustics, photodynamic, and photothermal therapy.[10a,12,15] In this current work, incorporation of PDA as a nanoparticle coating was confirmed visually by the gray to black color of the powder obtained after concentrating and washing the particles (Figure S2, Supporting Information). TEM imaging (Figure 1E) of the black residue, left after etching the $CaCO_3$ using hydrochloric acid (HCl), shows a collapsed polymer shell or film coating, which has similar FTIR absorption bands to the reference PDA film (Figure S1, Supporting Information).

The hybrid particles also exhibited a UV absorption maximum (λ_{max}) at 280 nm (Figure 1F), similar to previously reported PDA-mineralized vaterite[16] and another λ_{max} in the visible region at around 670 nm. Successful incorporation of PDA into the nanoparticles can be attributed to the adsorption of dopamine molecules to the surface of the $CaCO_3$ particles or via interactions of the calcium-binding catechol moieties of PDA with the Ca^{2+} in the mixture.[12,16]

2.2. Inhibition of Protein Corona Formation by Biomimetic Coating of the PDA/BSA/$CaCO_3$ Hybrid Particles

Red blood cell (RBC) membrane coating technology has been utilized in various materials, including mesoporous silica,[9a] gold,[17] iron oxide,[18] and upconversion nanoparticles[9b] as well as some microstructures like micromotors[9c] and robots.[19] Most of these works demonstrate that the RBC biomimetic coating can influence the degree of protein accumulation around coated materials that are intended for prolonging systemic circulation or circumventing immune responses to introduced materials. RBC membranes, shown in **Figure 2**A, are difficult to visualize compared to the original RBCs (Figure 2B) from which these membranes were derived. Figure 2C shows a schematic representation of the ultrasound-mediated technique for the RBC membrane coating of the hybrid particles. An initial confirmatory test for the success of RBC membrane coating of the hybrid particles was the comparison of the SDS–PAGE protein profiles (Figure 2D) of bare PDA/BSA/$CaCO_3$, the RBC membranes, and the RBC membrane-treated PDA/BSA/$CaCO_3$ hybrid particles. PDA/BSA/$CaCO_3$ hybrid particles alone have a prominent band between 50 and 75 kDa, corresponding to their BSA constituent. Additional bands, corresponding to the RBC membrane proteins (including spectrin, ankyrin, actin, glycophorin, and other membrane proteins),[20] after membrane coating treatment indicates that the hybrid particles were successfully incorporated into the RBC membranes. This was further supported by the resulting morphologies of particles, based on TEM imaging (Figure 2E) with almost unchanged hydrodynamic diameters before (571.62 ± 72.99 nm) and after RBC membrane coating (575.14 ± 30.73 nm). RBC membrane-coated PDA/BSA/$CaCO_3$ hybrid particles retain the general spherical shape of the hybrid particles, with the RBC membrane appearing as a thin coating, completely encapsulating the particles. Another observed effect of the RBC membrane coating is a slight change in the zeta potential of the hybrid particles, from −8.59 ± 2.19 to −10.71 ± 1.39 mV upon RBC

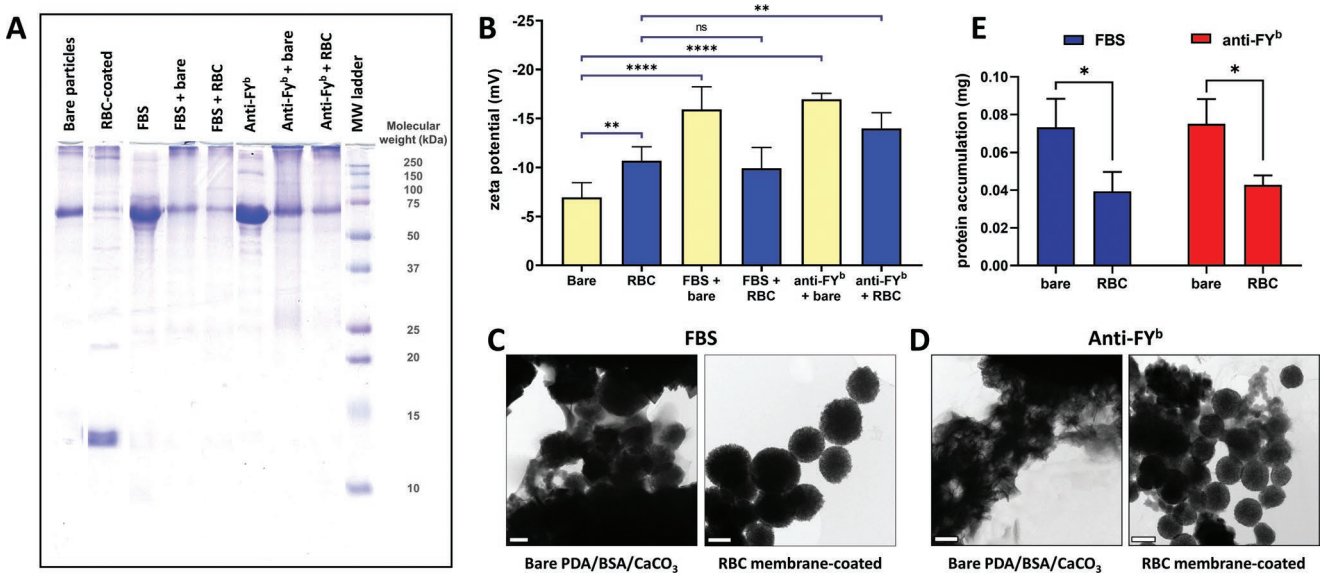

Figure 3. A) SDS–PAGE analysis showing the protein bands of bare PDA/BSA/$CaCO_3$, RBC membrane-coated PDA/BSA/$CaCO_3$, FBS, bare PDA/BSA/$CaCO_3$ and RBC membrane-coated PDA/BSA/$CaCO_3$ after incubation in FBS, anti-FY^b solution, bare PDA/BSA/$CaCO_3$ and RBC membrane-coated PDA/BSA/$CaCO_3$ after incubation in anti-FY^b solution, and standard protein molecular weight markers (MW ladder). B) A bar graph showing the zeta potentials of bare and RBC membrane-coated PDA/BSA/$CaCO_3$ particles, before and after incubation in the model protein solutions. Statistical differences by *t*-test are indicated by symbols over the lines above the bars: ns = not significant ($P > 0.05$), ** ($P \leq 0.01$), and **** ($P \leq 0.0001$). Transmission electron images showing the morphology of bare and RBC membrane-coated PDA/BSA/$CaCO_3$ hybrid particles after incubation C) in FBS and D) in anti-FY^b solution. Scale bar = 500 nm. E) A bar graph showing the amounts of protein accumulated by bare and RBC membrane-coated PDA/BSA/$CaCO_3$ particles before and after incubation in the model protein solutions. Statistical differences are indicated by asterisk over the lines above bars, where $P \leq 0.05$.

membrane coating. This indicates alterations in the surface composition and properties of the particles.

To demonstrate this projected effect of the RBC membrane coating on protein corona formation, hybrid particles with and without RBC membrane coating were incubated in protein model solutions, 10% fetal bovine serum (FBS), and anti-FY^b solution (containing 55% human blood plasma), to simulate their interactions with blood plasma proteins, and were then evaluated for hard protein corona formation. SDS–PAGE (**Figure 3**A) confirmed that the major protein contributor in the protein corona formation on both PDA/BSA/$CaCO_3$ and RBC membrane-coated PDA/BSA/$CaCO_3$ hybrid particles are proteins from the albumin family ($M_W \approx$ 50–70 kDa). This accumulation of the proteins around the hybrid particles also resulted in a significant change in the zeta potential of the bare PDA/BSA/$CaCO_3$ hybrid particles (Figure 3B). There was no significant change in the zeta potential of the RBC membrane-coated PDA/BSA/$CaCO_3$ hybrid particles after incubation in FBS; however, there is a slight but significant change ($P = 0.0087$) in its zeta potential after incubation in anti-FY^b solution. TEM images (Figure 3C,D) revealed that bare PDA/BSA/$CaCO_3$ hybrid particles appeared to have disintegrated, aggregated, or transformed into calcite particles after 4 h of incubation in FBS and anti-FY^b solution. Contrastingly, RBC membrane-coated PDA/BSA/$CaCO_3$ hybrid particles only had a slight change in morphology, including the formation of the protein coating as well as a small number of calcite particles. The amount of protein that formed the hard protein corona was quantified by Bradford assay (Figure 3E). After a 4 h incubation period, the amount of coronal proteins accumulated by the bare PDA/BSA/$CaCO_3$ hybrid particles in FBS and anti-FY^b solutions were 1.8 and 1.9 times higher than that of the RBC membrane-coated PDA/BSA/$CaCO_3$ hybrid particles, respectively.

2.3. Application of PDA/BSA/$CaCO_3$ Hybrid Particles as a pH-Responsive Ultrasound Contrast Agent

$CaCO_3$ particles are an extensively studied pH-responsive material, not only for their applicability for targeted delivery of active substances but also for their gas-generating capacity, which provides potential as an ultrasound contrast agent for the detection and imaging of tumor cells.[7b,21] These cells have slightly lower extracellular pH levels when compared to normal cells and this can trigger CO_2 production from local $CaCO_3$. To demonstrate the gas-generating, ultrasound contrast-enhancing capabilities of the bare and RBC membrane-coated PDA/BSA/$CaCO_3$ hybrid particles, we scanned dispersions of these particles in phosphate buffered saline (PBS) at different pH levels at different time points over 90 min. **Figure 4**A shows representative grayscale ultrasound images of cross-sectional areas of sample-loaded tubes. PBS without any of the hybrid particles at different pH and observation times showed very low ultrasound contrast, whereas dispersions containing the hybrid particles showed increasing visual contrast with decreasing pH levels.

To quantify the contrast enhancement brought about by the dispersions, the mean grayscale values of the ultrasonographs

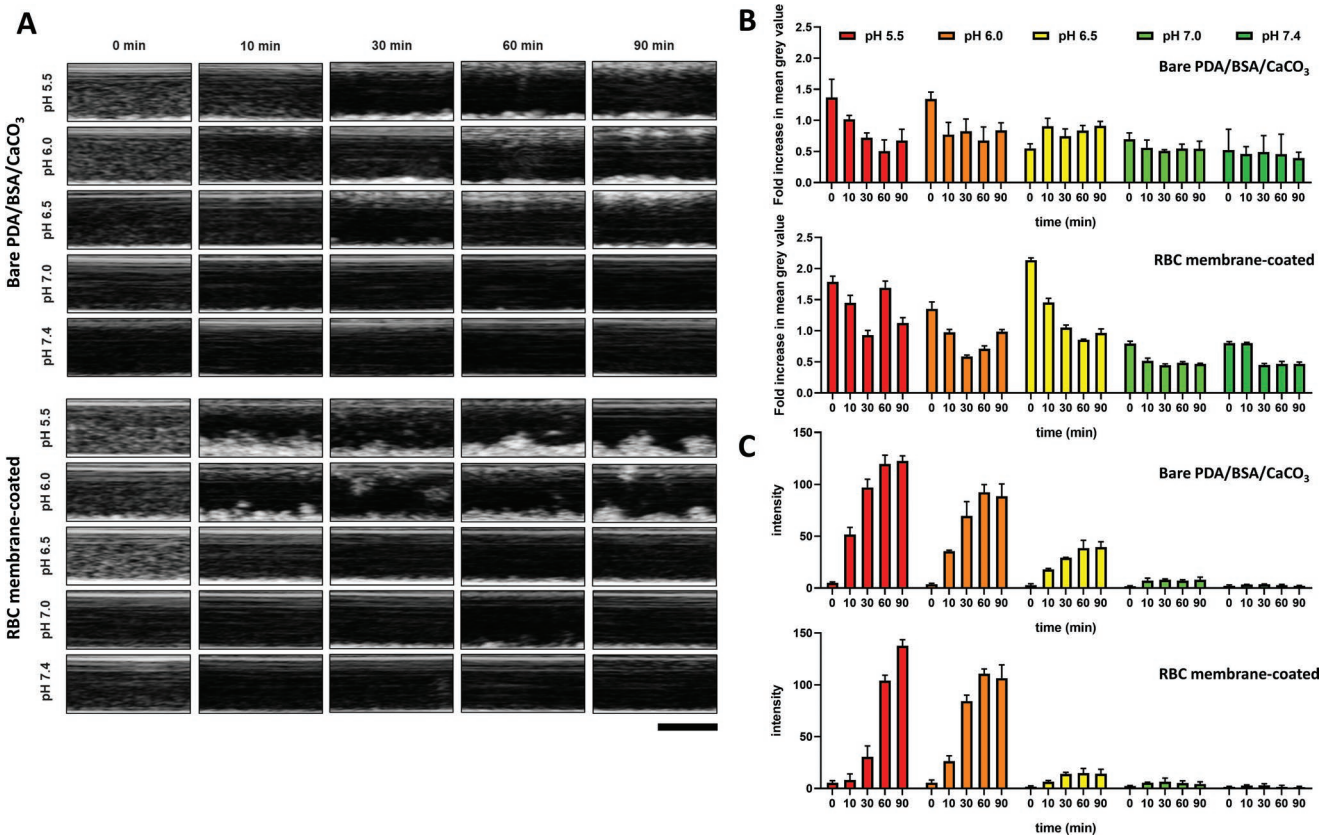

Figure 4. A) Representative ultrasonograms, and bar graphs showing B) the corresponding fold increase in the mean gray values of the images (compared to a PBS control) and C) the relative amounts of carbon dioxide produced by dispersions of bare and RBC membrane-coated PDA/BSA/$CaCO_3$ hybrid particles, in PBS at different pH levels, taken at different time points. Scale bar = 2.0 mm.

obtained were measured by digital image analysis. Figure 4B shows the fold increase in the mean gray values of the hybrid particle dispersions, relative to their respective blanks at different pH values. At all-time points, the normalized gray values of both bare and RBC membrane-coated PDA/BSA/$CaCO_3$ hybrid particles at pH 7.0 and 7.4 are significantly lower, compared to those at lower pH values. Bare hybrid particles at pH 6.5 had a gradual increase in gray value after 90 min; at pH 5.5 and 6.0, high ultrasound contrast was already observed upon dispersing the particles into the buffer, which decreased to about 15–25% of the original intensity over time. Similar trends were also observed with the normalized gray values of the RBC membrane-coated PDA/BSA/$CaCO_3$ hybrid particles over time; however, it was observed that the intensities of these coated particles at pH 5.5–6.5 were initially higher than those of the bare PDA/BSA/$CaCO_3$ hybrid particles. This observed difference in the contrast enhancement between the bare and coated hybrid particles might be due to the possibility that CO_2 can be entrapped and stabilized by the RBC membranes, and that additional contrast might arise from the RBC membranes (Figure S3, Supporting Information). The obtained gray values, however, decreased over time, reaching similar ultrasound contrast as the bare hybrid particles after 90 min, which can be attributed to the dissolution of CO_2. This indicates that the particles, upon exposure to a low pH environment (e.g., tumor extracellular conditions), can immediately affect contrast enhancement. Further, it is implied that the CO_2 produced is soluble in a physiological buffer, which is advantageous in the expulsion of the gas from a biological system.

To confirm that the visual contrast change and gray value enhancement by the dispersion of hybrid particles in response to decreased pH levels are indeed due to CO_2 generation, we monitored the CO_2 production at the same time points as when the ultrasonographs were taken. CO_2 was produced by the particles at all pH values; however, only small to negligible quantities of the gas were produced at pH 7.0 and 7.4 (Figure 4C). In addition, the amount and rate of production of CO_2 increased as the buffer pH decreased. The growth of CO_2 bubbles and separation or rising from the dispersion might explain why there is an inverse relationship between the CO_2 detected in the headspace and the ultrasound contrast over time at pH 5.5 and 6.0. Interestingly, CO_2 production was initially lower or delayed with the RBC membrane-coated PDA/BSA/$CaCO_3$ hybrid particles, despite the high ultrasound contrast observed at the same time point. Starting at 60 min, at pH 5.5 and 6.0 CO_2 levels produced by RBC membrane-coated PDA/BSA/$CaCO_3$ hybrid particles were comparable to those produced by the bare PDA/BSA/$CaCO_3$. Furthermore, at pH 6.5, CO_2 production by the coated hybrid particles was lower than

that by the bare hybrid particles. This implies that the RBC membrane coating might be acting as a barrier that can temporarily retain the produced CO_2 and/or delay or reduce the interactions between acidic environment and the hybrid particles.

2.4. Zebrafish Embryotoxicity Evaluation

In vivo biocompatibility of the PDA/BSA/$CaCO_3$ hybrid particles was evaluated using the fish embryo toxicity (FET) test under the guidelines of the organisation for economic co-operation and development (OECD).[22] Embryonic zebrafish are a popular vertebrate model organism due to: the optical transparency of the embryos, which permits easy observation of the occurring physiological processes; high fecundity of zebrafish that allows inexpensive analyses with high statistical reliability; and feasibility of transgenic modification to suit the intended purpose of the model.[23] The genetic, physiological, and pharmacological comparability of this model to humans makes it well suited for studying complex biological processes, including assessment of acute toxicity responses.

Figure 5A shows the survival rate of zebrafish embryos at different days after continuous treatment with PDA/BSA/$CaCO_3$ hybrid particles at varying concentrations. Negligible embryonic lethality was observed, and this was not significantly correlated with any treatment or control group. All of the surviving embryos showed normal gross morphology, depicted in Figure 5B, indicating that the PDA/BSA/$CaCO_3$ exhibits no demonstrable systemic toxicity in zebrafish embryos or larvae. This is in line with previous toxicity testing of PDA-containing and modified materials and related compounds in other vertebrate models.[24]

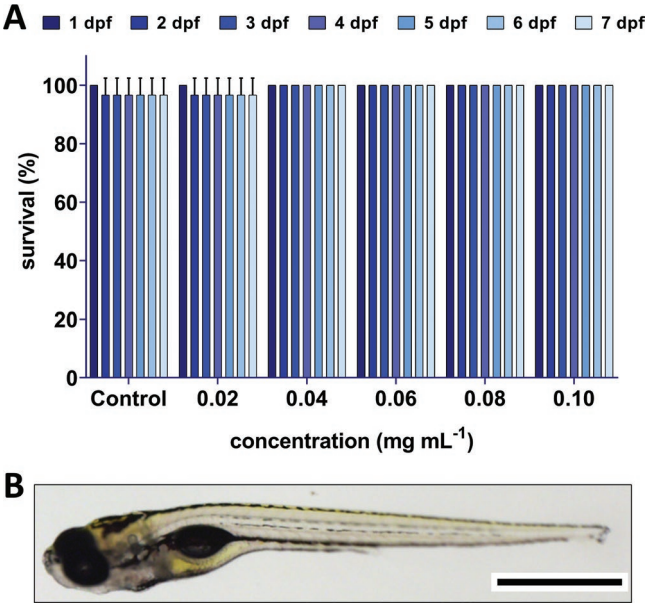

Figure 5. A) Bar graph showing the survival rate of zebrafish at different days postfertilization after treatment with different concentrations of PDA/BSA/$CaCO_3$. All values given are means from three experiments with $n = 10$. B) Image showing a zebrafish larvae at 7 dpf with normal gross morphology. Scale bar = 1.0 mm.

3. Conclusion

This current work demonstrates that hybrid particles from calcium carbonate, polydopamine, and bovine serum albumin exhibit pH responsiveness and ultrasound contrast enhancement. These properties indicate potential applications for noninvasive multimodal imaging for diagnosis and identification of tumor location, for photothermal and photodynamic therapy, and for active drug delivery applications. Furthermore, application of a biomimetic RBC membrane coating suggests the possibility of creating a "personalized" contrast agent and drug carrier system, with minimal alterations in surface properties due to inhibition of protein corona formation and with a reduced immune response elicited by administration of these particles.

4. Experimental Section

Materials: Calcium chloride dihydrate, sodium carbonate monohydrate, dopamine hydrochloride, BSA, sodium chloride, potassium chloride, disodium hydrogen phosphate, potassium dihydrogen phosphate, tris(hydroxymethyl)amino-methane hydrochloride (Tris), fetal bovine serum (FBS), Bradford reagent, and materials and reagents used for SDS–PAGE, such acrylamide, ammonium persulfate, SDS, *N,N,N′,N′*-tetramethyl-ethylenediamine, Coomassie brilliant blue, glycerol, and glycine, were purchased from Sigma-Aldrich (St. Louis, MO, USA) and used as received. Analytical reagent grade solvents such as ethanol and acetone were utilized in the study. Securacell reagent human red blood cells were used for membrane coating experiments. Parker Laboratories Aquasonic 100 Ultrasound Gel (ThermoFisher Scientific) was used for ultrasound imaging.

Preparation of PDA/BSA/$CaCO_3$ Hybrid Particles: Hybrid particles were fabricated using a combination of methods, based on the reports of Mallampati and Valiyaveettil,[25] and Kim and Park.[16] A mixture containing 16.0 mg dopamine hydrochloride, 16.4 mg $Na_2CO_3{\cdot}2H_2O$, and 4.00 mL Tris buffer (10 mmol L^{-1}, pH 8.5) was magnetically stirred for 10 min, yielding a light brown dispersion. The brown mixture was added to a solution of 4.00 mL Tris buffer (10 mmol L^{-1}, pH 8.5), 36.0 mg BSA, and 20 mg $CaCl_2{\cdot}2H_2O$. The resulting mixture was stirred for 3 min to yield a light brown dispersion. The dispersion was concentrated by centrifugation at 6000 × *g* for 2 min and washed sequentially with water, ethanol, and acetone, prior to drying. The resulting powder was stored at 4 °C until further use.

Preparation of RBC Membranes and RBC Membrane-Coated PDA/BSA/$CaCO_3$ Hybrid Particles: Preparation of the RBC membranes was a modification of the method reported by Himbert et al.[26] From a 2 mL reagent red blood cell sample, RBCs were concentrated by centrifugation at 3000 × *g* for 10 min at room temperature. The simulated blood plasma layer was pipetted out of the tube and the remaining pellet was washed thrice with 10 mL isotonic PBS (pH 7.4) by centrifugation at 3000 × *g* for 10 min at room temperature. The RBC-containing pellet (≈0.5 mL) was then mixed with 10 mL hypotonic PBS (pH 7.4). This mixture was vortexed for 10 s to prevent clumping and then placed immediately in an ice bath for 30 min to slow down the reclosing of the ruptured cell membranes. The mixture was then centrifuged at 6000 × *g* for 20 min. The resulting supernatant was removed and the remaining pellet was reconstituted in 10 mL of hypotonic PBS (pH 7.4). The mixture was vortexed for 10 s and then centrifuged at 6000 × *g* for 20 min. This process of removal of the supernatant and recentrifugation was repeated twice, yielding the RBC membranes as a pink pellet. This pellet was washed three times with isotonic PBS (pH 7.4). In order to coat the hybrid particles with RBC membranes, 10 µL RBC membrane-containing PBS solution was mixed with 1.0 mL hybrid particle dispersion (1.0 mg mL^{-1}) in isotonic PBS and then insonated in an ultrasonic bath for 10 min.

Physicochemical Characterization of Bare and RBC Membrane-Coated PDA/BSA/CaCO3 Hybrid Particles– Optical Properties: UV–vis spectra of the hybrid particles were obtained using a Cary 60 UV–vis spectrophotometer (Agilent Technologies). Fourier transform infrared spectra of dopamine hydrochloride, BSA, PDA, and the hybrid particles were taken using a Cary 630 FTIR spectrometer fitted with the monolithic design diamond attenuated total reflectance accessory (Agilent Technologies).

Dynamic Light Scattering and Phase Analysis Light Scattering: Hydrodynamic diameters and zeta potentials of the particles were determined by DLS and PALS, respectively, using a Brookhaven NanoBrook Omni particle sizer and zeta potential analyzer.

Polymorph Identification by Powder X-Ray Diffractometry: $CaCO_3$ polymorphs present in the particles were identified by their X-ray diffraction patterns, gathered using a Bruker D8 Advance Eco X-ray powder diffractometer with a Cu K_α radiation, running at 40 kV and 25 mA.

Analysis of Particle Size and Morphology by Transmission Electron Microscopy: Particle size and morphology of the hybrid particles were studied using transmission electron microscopy (FEI Tecnai T20 TEM). Samples were prepared by drop casting 3.0 µL aliquots of the particle dispersions onto holey carbon film-coated, 300 mesh copper grids (EM Solutions), which were then air dried for at least an hour, prior to analysis.

Protein Profiling by SDS–PAGE: Protein profiles of the RBC membranes, hybrid particles, and RBC membrane-coated hybrid particles were studied using the 12% denaturing SDS–PAGE method.

In vitro Protein Corona Studies: Protein corona formation on the synthesized bare and RBC membrane-coated PDA/BSA/$CaCO_3$ hybrid particles was explored using a method similar to that described by Rao et al.[9b] An isotonic PBS (pH 7.4) mixture containing 1.0 mg mL^{-1} particles and the model protein solution was mixed for 4 h at room temperature, then centrifuged and washed with isotonic PBS (pH 7.4). Model protein solutions used in the experiments were 10.0 mg mL^{-1} FBS, and anti-FY^a solution (Immucor, Inc.), containing 55% human blood plasma. The resulting pellets were saved for analysis. Changes in the particle size and zeta potential were evaluated using DLS and PALS, respectively. Changes in particle morphology were studied using TEM. Protein profile and contents of the untreated particles, and corona-coated particles were determined using 12% denaturing SDS–PAGE and Bradford assay.[27]

Ultrasound and pH Response Evaluation: To quantify the ultrasound contrast that may arise from the particles, dispersions of the particles (4.0 mg mL^{-1}) in PBS at different pH levels (5.5, 6.0, 6.5, 7.0, and 7.4) were loaded into 5.0 cm polyethylene tubes (2.0 and 3.0 mm inner and outer diameter, respectively). The tubes, embedded in a lump of ultrasound gel on a paraffin platform, were imaged using a Vevo 2100 Ultrahigh Frequency ultrasound scanner with a 40 MHz ultrasound transducer at different time points for 90 min. Ultrasound images were recorded and processed into grayscale images for quantitative image analysis using ImageJ.[28]

To evaluate the CO_2-generating capacity of the hybrid particles, dispersions of the hybrid particles in PBS at different pH values (4.0 mg mL^{-1}, 300 µL) were placed into 2 mL vials with bonded-in polytetrafluoroethylene/silicone septa. Carbon dioxide gas, generated in the headspace, was monitored by gas chromatography using an Agilent 7890A gas chromatography (GC) system, coupled with a thermal conductivity detector. Chromatographic separation was performed using an HP-PLOT Molesieve GC column (Agilent). Helium was used as carrier gas (99.999% purity) at a constant flow rate of 3.0 mL min^{-1}. The chromatographic conditions were: oven temperature program, 150 °C (hold 1.50 min); injector temperature, 120 °C; injection volume, 100 µL; and split ratio, 10:1.

Zebrafish Embryo Toxicity Assay: All experiments using zebrafish were assessed and approved by the Monash University Animal Ethics Committee and were conducted under applicable Australian laws governing the care and use of animals for scientific research. Wild type zebrafish (*Danio rerio*) embryos from the Tübingen strain were collected immediately after fertilization and were maintained according to standard protocols[29] until 24 h postfertilization (hpf). Embryos were then manually dechorionated and subjected to 3.0 mL of selected treatment with PDA/BSA/$CaCO_3$ particles in E3 media or E3 media alone as a control solution in a six-well plate (n = 10 embryos per well). Tested concentrations of PDA/BSA/$CaCO_3$ were 20, 40, 60, 80, and 100 µg mL^{-1}. Embryonic/larval survival was scored daily from 48 hpf to 7 d postfertilization (dpf), as were the presence of any gross morphological abnormalities at these time points.

Statistical Analyses: Statistical tests, including t-test and two-way analysis of variance followed by Tukey's multiple comparisons test, were performed using GraphPad Prism version 8.0.0 for Windows, GraphPad Software, San Diego, California, USA, www.graphpad.com

Supporting Information

Supporting Information is available from the Wiley Online Library or from the author.

Acknowledgements

The authors acknowledge use of facilities within the Monash Centre for Electron Microscopy, Monash Biomedical Imaging, and Monash X-ray Platform. The authors also acknowledge the assistance of Prof. Gil Garnier (BioResource Processing Research Institute of Australia, Department of Chemical Engineering, Monash University), Dr. Timothy Williams (Monash Centre for Electron Microscopy), Dr. Ekaterina Salimova (Monash Biomedical Imaging), Dr. Manuel Pumarol Crestar (School of Physics, Monash University), Dr. Ruby Law (Department of Biochemistry and Molecular Biology, Monash University), and Maria Triantis (School of Chemistry, Monash University). The authors thank the technical staff from the AquaCore facility, Monash University, for their expertise in handling and maintenance of zebrafish. The Australian Regenerative Medicine Institute is supported by grants from the State Government of Victoria and the Australian Government.

Conflict of Interest

The authors declare no conflict of interest.

Keywords

calcium carbonate nanoparticles, contrast enhanced ultrasound imaging, protein corona, red blood cell membranes

Received: November 26, 2019
Revised: January 1, 2020
Published online:

[1] a) Y. Xie, J. Wang, Z. Wang, K. A. Krug, J. D. Rinehart, *Nanoscale* **2018**, *10*, 12813; b) C. Barsanti, F. Lenzarini, C. Kusmic, *World J. Diabetes* **2015**, *6*, 792.
[2] E. Stride, N. Saffari, *Proc. Inst. Mech. Eng., Part H* **2003**, *217*, 429.
[3] a) J. R. Eisenbrey, A. Sridharan, J.-B. Liu, F. Forsberg, *Biomed. Res. Int.* **2015**, *2015*, 1; b) K. Hoyt, A. Sorace, R. Saini, *Invest. Radiol.* **2012**, *47*, 167.
[4] F. Calliada, R. Campani, O. Bottinelli, A. Bozzini, M. G. Sommaruga, *Eur. J. Radiol.* **1998**, *27*, S157.
[5] a) F. Günther, T. Heidt, M. Kramer, E. Khanicheh, A. L. Klibanov, A. Geibel-Zehender, E. A. Ferrante, I. Hilgendorf, D. Wolf, A. Zirlik,

J. Reinöhl, C. Bode, K. Peter, B. A. Kaufmann, C. v. z. Mühlen, *Sci. Rep.* **2017**, *7*, 14898; b) X. Liu, P. Gong, P. Song, F. Xie, A. L. Miller Ii, S. Chen, L. Lu, *Polym. Chem.* **2019**, *10*, 705; c) X. Liu, P. Gong, P. Song, F. Xie, A. L. Miller Ii, S. Chen, L. Lu, *Biomater. Sci.* **2018**, *6*, 623; d) S. Unnikrishnan, A. L. Klibanov, *Am. J. Roentgenol.* **2012**, *199*, 292.

[6] M. Ma, H. Chen, J. Shi, *Sci. Bull.* **2015**, *60*, 1170.

[7] a) Q. Feng, W. Zhang, X. Yang, Y. Li, Y. Hao, H. Zhang, L. Hou, Z. Zhang, *Adv. Healthcare Mater.* **2018**, *7*, 1700957; b) K. H. Min, H. S. Min, H. J. Lee, D. J. Park, J. Y. Yhee, K. Kim, I. C. Kwon, S. Y. Jeong, O. F. Silvestre, X. Chen, Y.-S. Hwang, E.-C. Kim, S. C. Lee, *ACS Nano* **2015**, *9*, 134.

[8] M. Rahman, S. Laurent, N. Tawil, L. Yahia, M. Mahmoudi, in *Protein-Nanoparticle Interactions*, Vol. *15*, Springer, Berlin, Heidelberg **2013**.

[9] a) M. Xuan, J. Shao, J. Zhao, Q. Li, L. Dai, J. Li, *Angew. Chem., Int. Ed.* **2018**, *57*, 6049; b) L. Rao, Q.-F. Meng, L.-L. Bu, B. Cai, Q. Huang, Z.-J. Sun, W.-F. Zhang, A. Li, S.-S. Guo, W. Liu, T.-H. Wang, X.-Z. Zhao, *ACS Appl. Mater. Interfaces* **2017**, *9*, 2159; c) Z. Wu, T. Li, J. Li, W. Gao, T. Xu, C. Christianson, W. Gao, M. Galarnyk, Q. He, L. Zhang, J. Wang, *ACS Nano* **2014**, *8*, 12041.

[10] a) D. L. Longo, R. Stefania, S. Aime, A. Oraevsky, *Int. J. Mol. Sci.* **2017**, *18*, 1719; b) M. d'Ischia, A. Napolitano, V. Ball, C.-T. Chen, M. J. Buehler, *Acc. Chem. Res.* **2014**, *47*, 3541.

[11] S. Maleki Dizaj, M. Barzegar-Jalali, M. H. Zarrintan, K. Adibkia, F. Lotfipour, *Expert Opin. Drug Delivery* **2015**, *12*, 1649.

[12] Z. Dong, L. Feng, Y. Hao, M. Chen, M. Gao, Y. Chao, H. Zhao, W. Zhu, J. Liu, C. Liang, Q. Zhang, Z. Liu, *J. Am. Chem. Soc.* **2018**, *140*, 2165.

[13] Y. Liu, Y. Chen, X. Huang, G. Wu, *Mater. Sci. Eng., C* **2017**, *79*, 457.

[14] D. B. Trushina, T. V. Bukreeva, M. V. Kovalchuk, M. N. Antipina, *Mater. Sci. Eng., C* **2014**, *45*, 644.

[15] a) Y. Wang, X. Pang, J. Wang, Y. Cheng, Y. Song, Q. Sun, Q. You, F. Tan, J. Li, N. Li, *J. Mater. Chem. B* **2018**, *6*, 2460; b) Y. Li, C. Jiang, D. Zhang, Y. Wang, X. Ren, K. Ai, X. Chen, L. Lu, *Acta Biomater.* **2017**, *47*, 124; c) X. Zhang, X. Nan, W. Shi, Y. Sun, H. Su, Y. He, X. Liu, Z. Zhang, D. Ge, *Nanotechnology* **2017**, *28*, 295102; d) H. Zhuang, H. Su, X. Bi, Y. Bai, L. Chen, D. Ge, W. Shi, Y. Sun, *ACS Biomater. Sci. Eng.* **2017**, *3*, 1799.

[16] S. Kim, C. B. Park, *Langmuir* **2010**, *26*, 14730.

[17] W. Gao, C.-M. J. Hu, R. H. Fang, B. T. Luk, J. Su, L. Zhang, *Adv. Mater.* **2013**, *25*, 3549.

[18] L. Rao, L.-L. Bu, J.-H. Xu, B. Cai, G.-T. Yu, X. Yu, Z. He, Q. Huang, A. Li, S.-S. Guo, W.-F. Zhang, W. Liu, Z.-J. Sun, H. Wang, T.-H. Wang, X.-Z. Zhao, *Small* **2015**, *11*, 6225.

[19] B. E.-F. de Ávila, P. Angsantikul, D. E. Ramírez-Herrera, F. Soto, H. Teymourian, D. Dehaini, Y. Chen, L. Zhang, J. Wang, *Sci. Rob.* **2018**, *3*, eaat0485.

[20] Y. Lu, J. Liu, *Front. Biol. (Beijing, China)* **2007**, *2*, 247.

[21] M. Kim, J. H. Lee, S. E. Kim, S. S. Kang, G. Tae, *ACS Appl. Mater. Interfaces* **2016**, *8*, 8409.

[22] OECD, *Test No. 236: Fish Embryo Acute Toxicity (FET) Test*, OECD Publishing, Paris **2013**, https://doi.org/10.1787/9789264203709-en.

[23] K. Y. Lee, G. H. Jang, C. H. Byun, M. Jeun, P. C. Searson, K. H. Lee, *Biosci. Rep.* **2017**, *37*, BSR20170199.

[24] a) X. Liu, J. Cao, H. Li, J. Li, Q. Jin, K. Ren, J. Ji, *ACS Nano* **2013**, *7*, 9384; b) S. Hong, K. Y. Kim, H. J. Wook, S. Y. Park, K. D. Lee, D. Y. Lee, H. Lee, *Nanomedicine* **2011**, *6*, 793; c) K.-Y. Ju, Y. Lee, S. Lee, S. B. Park, J.-K. Lee, *Biomacromolecules* **2011**, *12*, 625.

[25] R. Mallampati, S. Valiyaveettil, *RSC Adv.* **2015**, *5*, 11023.

[26] S. Himbert, R. J. Alsop, M. Rose, L. Hertz, A. Dhaliwal, J. M. Moran-Mirabal, C. P. Verschoor, D. M. E. Bowdish, L. Kaestner, C. Wagner, M. C. Rheinstädter, *Sci. Rep.* **2017**, *7*, 39661.

[27] M. M. Bradford, *Anal. Biochem.* **1976**, *72*, 248.

[28] C. A. Schneider, W. S. Rasband, K. W. Eliceiri, *Nat. Methods* **2012**, *9*, 671.

[29] M. Westerfield, *The Zebrafish Book. A Guide for the Laboratory Use of Zebrafish (Danio Rerio)*, Univ. of Oregon Press, Eugene, Oregon **2000**.

